Title

Ex situ metrology and data analysis for optimization of beamline performance of aspherical pre-shaped x-ray mirrors at the advanced light source

Journal

Review of Scientific Instruments, 90(2)

ISSN

0034-6748

Authors

Yashchuk, Valeriy V

Lacey, Ian

Gevorkyan, Gevork S

et al.

Publication Date

2019-02-01

DOI

10.1063/1.5057441

Peer reviewed

Review of Scientific Instruments

Ex situ metrology and data analysis for optimization of beamline performance of aspherical pre-shaped x-ray mirrors at the advanced light source

Cite as: Rev. Sci. Instrum. **90**, 021711 (2019); https://doi.org/10.1063/1.5057441
Submitted: 14 September 2018 . Accepted: 17 January 2019 . Published Online: 15 February 2019

Valeriy V. Yashchuk, Ian Lacey, Gevork S. Gevorkyan, Wayne R. McKinney, Brian V. Smith, and Tony Warwick

Review of Scientific Instruments ARTICLE scitation.org/journal/rsi

Ex situ metrology and data analysis for optimization of beamline performance of aspherical pre-shaped x-ray mirrors at the advanced light source

Cite as: Rev. Sci. Instrum. 90, 021711 (2019); doi: 10.1063/1.5057441
Submitted: 14 September 2018 • Accepted: 17 January 2019 •
Published Online: 15 February 2019

Valeriy V. Yashchuk,[1,a)] Ian Lacey,[1] Gevork S. Gevorkyan,[1,b)] Wayne R. McKinney,[1] Brian V. Smith,[2] and Tony Warwick[1]

AFFILIATIONS

[1]Advanced Light Source, Lawrence Berkeley National Laboratory, Berkeley, California 94720, USA
[2]Engineering Division, Lawrence Berkeley National Laboratory, Berkeley, California 94720, USA

[a)]**Electronic mail:** vvyashchuk@lbl.gov.
[b)]This research was performed while G. S. Gevorkyan was at the Advanced Light Source, Lawrence Berkeley National Laboratory, Berkeley, CA 94720, USA.

ABSTRACT

Super high quality aspherical x-ray mirrors with a residual slope error of ~100 nrad (root-mean-square) and a height error of ~1-2 nm (peak-to-valley), and even lower, are now available from a number of the most advanced vendors utilizing deterministic polishing techniques. The mirror specification for the fabrication is based on the simulations of the desired performance of the mirror in the beamline optical system and is normally given with the acceptable level of deviation of the mirror figure and finish from the desired ideal shape. For example, in the case of aspherical x-ray mirrors designed for the Advanced Light Source (ALS) QERLIN beamline, the ideal shape is defined with the beamline application (conjugate) parameters and their tolerances. In this paper, we first discuss an original procedure and dedicated software developed at the ALS X-Ray Optics Laboratory (XROL) for optimization of beamline performance of pre-shaped hyperbolic and elliptical mirrors. The optimization is based on results of *ex situ* surface slope metrology and consists in minimization of the mirror shape error by determining the conjugate parameters of the best-fit ideal shape within the specified tolerances. We describe novel optical metrology instrumentation, measuring techniques, and analytical methods used at the XROL for acquisition of surface slope data and optimization of the optic's beamline performance. The high efficacy of the developed experimental methods and data analysis procedures is demonstrated in results of measurements with and performance optimization of hyperbolic and elliptical cylinder mirrors designed and fabricated for the ALS QERLIN beamline.

I. INTRODUCTION

The development of fully coherent free electron lasers and diffraction limited storage ring x-ray sources has brought to a focus the need for higher performing x-ray optics with unprecedented tolerances for surface slope and height errors and roughness.[1–5] For example, the proposed beamlines for the future upgraded Advanced Light Source, ALS-U,[6,7] require mirrors characterized by a residual slope error of <100 nrad (root-mean-square, RMS) and a height error of <1-2 nm (peak-to-valley, PV). Such high quality aspherical x-ray mirrors are now available from a number of the most advanced vendors utilizing deterministic polishing techniques. For fabrication, the vendors usually use unique surface metrology tools

and data processing algorithms, generally developed on site, that are not available in the optical metrology labs at x-ray facilities.

The mirror specification for fabrication is generally based on simulations of the desired performance of the mirror in the beamline optical system and is normally given with the acceptable level of deviation of the mirror figure and finish from the desired ideal shape. In the case of an aspherical x-ray mirror, the ideal shape is usually defined with the beamline application (conjugate) parameters (distances from the source and image focal points to the mirror center and the corresponding grazing incidence angles) and, more recently, with tolerances for the parameters.

To fully exploit the potential of the optics at the beamlines, we need *ex situ* metrology methods and tools able to characterize the optics with accuracy even better than the optical specification (see, for example, Ref. 8 and references therein). Besides measuring mirrors to ensure vendor compliance to specifications, the role of *ex situ* metrology at an x-ray facility is to assure the quality of the optical components mounted on a steerable support, installed in beamlines, and used as a part of the experimental systems.

In this paper, we present the results of our recent work at the ALS X-Ray Optics Laboratory (XROL)[9,10] developing novel optical metrology instrumentation, measuring techniques, and methods for data acquisition and analysis. We initially discuss an original procedure and dedicated software developed at the XROL for optimization of the beamline performance of pre-shaped hyperbolic and elliptical mirrors. The optimization makes the most of the results of *ex situ* surface slope metrology and consists in minimization of the mirror shape error by determining the conjugate parameters of the best-fit ideal shape within the specified tolerances. The determined optimal conjugate parameters completely define the optimal alignment of the mirror at the beamline that effectively preserves the desired shape of the mirror.

The high efficacy of the developed measurement and data analysis procedures is demonstrated by results of measurements and performance optimization of hyperbolic (SM1) and elliptical (SM2) cylinder mirrors fabricated for the ALS QERLIN beamline.[11] For surface slope metrology with the mirrors, we used the Developmental Long Trace Profiler (DLTP)[12–14] and verified the results via comparison with that of obtained with the new Optical Surface Measuring System (OSMS),[15–17] both available at the ALS XROL.

The paper is organized as follows. In Sec. II, we first discuss the specification of the hyperbolic and elliptical cylinder mirrors SM1 and SM2 designed for usage in the Wolter optical system[18,19] of the QERLIN spectrometer.[11] The specification is given in the terms of the mirror's conjugate parameters and their tolerances. Therefore, we next present the analytical expressions describing the tangential surface slope and height profiles of the ideal hyperbolic and elliptical cylinder mirrors as functions of their conjugate parameters. In Sec. III, we present the results of high accuracy surface slope metrology with the QERLIN hyperbolic and elliptical mirrors carried out at the ALS XROL. In both cases, the measured surface figures significantly deviate from the ideal shapes evaluated using the derived analytical expressions with the specified central values of the conjugate parameters. A question naturally arises whether the measured surface shapes of the optics correspond to the desired shapes given by the conjugate parameters with the tolerances. In order to answer that question, in Sec. IV, we briefly review the mathematical foundations of the method of characteristic functions[18–20] developed at the XROL for *ex situ* optimal tuning of bendable optics. Here, such methods have been extended to determine the optimal conjugate parameters of a pre-shaped mirror. The optimal conjugate parameters correspond to the ideal shape that best-fits the shape measured by *ex situ* metrology with the mirror. Realization of the developed analytical methods in dedicated software has been applied to optimize the conjugate parameters of the QERLIN SM1 and SM2 mirrors, as discussed and demonstrated in Sec. IV. We conclude (Sec. V) with a discussion of the obtained results and statement of the planned work on the further development of the method and software to account in the optimization of the peculiarities of mirror applications such as non-uniform distribution of intensity of the incident x-ray beam.[20]

II. SURFACE FIGURE OF HYPERBOLIC AND ELLIPTICAL CYLINDER X-RAY MIRRORS IN TERMS OF THE CONJUGATE PARAMETERS

A. Tolerance specification of pre-shaped x-ray mirrors and new challenges for *ex situ* metrology

The QERLIN beamline[11] under construction at the ALS is a Double-Dispersion Resonance Inelastic X-ray Scattering (RIXS) beamline. The high-resolution RIXS technique allows probing the electronic excitations of complex materials with unprecedented precision.[21] Similar beamlines are in operation at the HZB/BESSY-II (Germany)[22] and under construction at MAX-IV (Sweden)[23] and TPS (Taiwan).[24] The RIXS process has a low cross section, compounded by the fact that the optical spectrometers used to analyze the scattered photons can only collect a small solid angle and have low efficiency. A significant increase in the throughput of RIXS systems can be achieved by application of energy multiplexing so that a complete RIXS map of scattered intensity versus photon energy in, and photon energy out, can be recorded simultaneously.[20] In the case of the ALS QERLIN beamline, this parallel acquisition scheme should provide a gain in throughput of over 100.[11]

The QERLIN spectrometer includes three aspherically pre-shaped mirrors. The vertically deflecting hyperbolic (SM1) and elliptical (SM2) mirrors constitute a Walter Type I optical schematic (Fig. 1) allowing the construction of a relatively short spectrometer with minimized aberration due to a long vertical focal length. A horizontally deflecting elliptical mirror (SM3) focuses x-rays in the horizontal plane.

The mirror substrates made of single-crystal silicon have overall dimensions of 160 (length) × 50 (width) × 50 (thickness) mm^3 with clear apertures (CA) of 150 mm × 20 mm for SM1 and SM2 mirrors, and 300 × 50 × 75 mm^3 with a CA of 290 mm × 20 mm for the SM3 mirror.

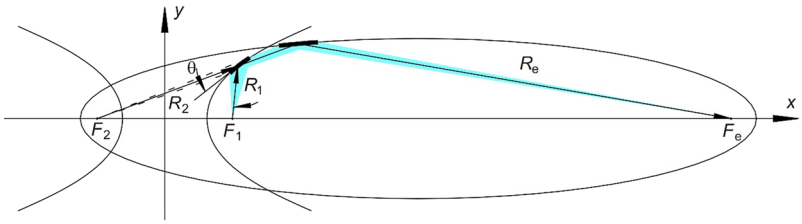

FIG. 1. The Wolter Type I optical system consisting of a pair of mirrors, one hyperbolic and one elliptical. F_1 is the object focus of the hyperbolic mirror, F_2 is the common focus of the mirrors, F_e is the image focus of the elliptical mirror, R_2 is the distance from the virtual focus F_2 to the center of the hyperbolic mirror, R_e is the distance from the elliptical mirror's center and the system focus (image position) F_e, and θ is the grazing incidence angle at the hyperbolic mirror's center.

The mirrors have been fabricated using a deterministic polishing process with the goal to match the desired shape determined by the conjugate parameters specified with the corresponding tolerances, as depicted in Table I. For all three mirrors, the residual, after subtraction of the best-fit desired shape within the specified tolerances, must have surface slope errors less than 150 nrad (RMS).

Such a specification of the mirrors for the QERLIN spectrometer sets new challenges for *ex situ* metrology. It is not enough just to measure the optics with required accuracy and compare the result with the unique desired shapes. We should be able to process the measured data and determine the optimal conjugate parameters, corresponding to the desired hyperbolic or elliptical topology that best fits the measured surface figure. A criterion for acceptance of the best-fit parameters is their satisfaction to the specified tolerances.

B. Description of hyperbolic cylinder mirror in the terms of the conjugate parameters

Practically speaking, the fabrication, assembly, and measurement of mirror shapes are performed in the rotated, mirror-related coordinate (MRC) system centered in the mirror center and with the tangential axis directed along the tangent of the mirror center.

The basic equations describing the distributions of the tangential surface height, slope, and local radius of curvature of a hyperbolic cylinder x-ray mirror in the MRC system and expressed in terms of the mirror conjugate parameters R_1, R_2, and θ (Fig. 2) have been derived and thoroughly examined in report[25] that is available upon direct request. Below, we present the major results of the derivations needed for the topics under discussion in this paper. In order to be in accordance with the definitions in Ref. 25, R_1 and R_2 are positive scalars.

TABLE I. Conjugate parameters specified for the QERLIN spectrometer mirrors.

Mirror	R_{SM}[a] (mm)	ΔR_{SM}[b] (mm)	R_{MI}[a] (mm)	ΔR_{MI}[b] (mm)	θ[c] (deg)	$\Delta\theta$[c] (deg)
SM1	700.00	±10	1781.97	±10	2.00	±0.03
SM2	1981.97	±10	3600.00	±10	2.00	±0.03
SM3	1200.00	±10	3288.18	±10	2.00	±0.03

[a] R_{SM} and R_{MI} are the specified center values of the source-to-mirror and mirror-to-image distances.
[b] ΔR_{SM} and ΔR_{MI} are the tolerances specified for the source-to-mirror and mirror-to-image distances.
[c] θ and $\Delta\theta$ are the central value of the grazing incidence angle and its tolerance in degrees.

The derivations comprise a sequential transition from the canonical description of hyperbola geometry with the general equation,

$$\frac{x^2}{a^2} - \frac{y^2}{b^2} = 1, \tag{1}$$

(where a and b are the major real and "imaginary" semi-axes of the hyperbola, $a = (R_2 - R_1)/2$ and $b = \sin\theta\sqrt{R_2 R_1}$), given in the canonical coordinate system to the description via the conjugate parameters in the MRC system (x_R, y_R)–Fig. 2.

First, the canonical coordinate system (x, y) in Fig. 2 is shifted in the vertical and horizontal directions, $(\tilde{x}, \tilde{y}) = (x + X_0, y + Y_0)$, placing the mirror center (pole) given in the canonical system with coordinates (X_0, Y_0),

$$X_0 = \frac{R_2^2 - R_1^2}{2\sqrt{R_2^2 + R_1^2 - 2R_2R_1\cos(2\theta)}}, \tag{2a}$$

$$Y_0 = \frac{R_2R_1\sin(2\theta)}{\sqrt{R_2^2 + R_1^2 - 2R_2R_1\cos(2\theta)}}, \tag{2b}$$

to the center of the $(\tilde{x}, \tilde{y})$ coordinate system. In the shifted system, the hyperbola equation (1) transforms to

$$\tilde{y}(\tilde{x}) = b\sqrt{\frac{(\tilde{x} + X_0)^2}{a^2} - 1} - Y_0, \tag{3}$$

with the angle β between the tangent of the mirror pole and the $\tilde{x}$-axis given by

$$\beta = \arctan\left[\frac{(R_2 + R_1)\tan\theta}{R_2 - R_1}\right]. \tag{4}$$

Next, we apply rotation transformation with angle $-\beta$ to the hyperbola in (3),

$$x_R(\tilde{x}) = \tilde{x}\cos\beta + \tilde{y}(\tilde{x})\sin\beta, \tag{5a}$$

$$y_R(\tilde{x}) = \tilde{y}(\tilde{x})\cos\beta - \tilde{x}\sin\beta. \tag{5b}$$

Technically, the transformations (3) and (5) with all parameters expressed via the mirror conjugate parameters are performed using the analytical capabilities of Mathematica™ software (version 11.1.1). The resultant expressions for $x_R(\tilde{x})$ and $y_R(\tilde{x})$ are

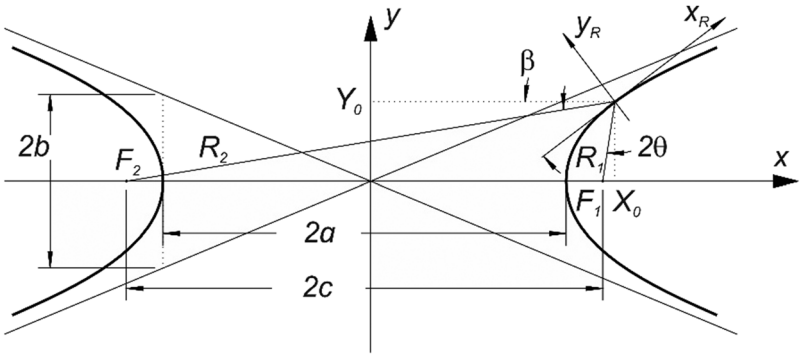

FIG. 2. Hyperbola geometry and the major parameters used in the derivations. β is the angle between *x*-axis of the canonic coordinate system of the hyperbola and the tangent of the mirror center with the coordinates (X_0, Y_0). Axes $\vec{x}_R$ and $\vec{y}_R$ define the mirror-related Cartesian coordinate system; *a* and *b* are the major real and "imaginary" semi-axes of the hyperbola. R_1 and R_2 are positive scalars.

$$x_R(\tilde{x}) = \frac{(R_2 - R_1)^2 x + (R_2 + R_1)\left[\sqrt{R_1R_2}\sqrt{(4(x + X_0)^2 - (R_2 - R_1)^2}\sin\theta - (R_2 - R_1)Y_0\right]\tan\theta}{(R_2 - R_1)\sqrt{(R_2 - R_1)^2 + (R_2 + R_1)^2\tan^2\theta}}, \tag{6a}$$

$$y_R(\tilde{x}) = \frac{\sqrt{R_1R_2}\sqrt{4(\tilde{x} + X_0)^2 - (R_2 - R_1)^2}\sin\theta - (R_2 - R_1)Y_0 - \tilde{x}(R_2 + R_1)\tan\theta}{\sqrt{(R_2 - R_1)^2 + (R_2 + R_1)^2\tan^2\theta}}. \tag{6b}$$

The tangential surface slope distribution $\alpha_R(\tilde{x})$ for the hyperbolic mirror in the MRC system is derived by direct differentiation of Eqs. (6a) and (6b),

$$\tan\alpha_R(\tilde{x}) = \frac{dy_R(\tilde{x}(x_R))}{dx_R} = \frac{dy_R(\tilde{x})}{d\tilde{x}} \cdot \left(\frac{dx_R(\tilde{x})}{d\tilde{x}}\right)^{-1}. \tag{7}$$

This leads to the following expression for the surface slope distribution for the hyperbolic mirror:

$$\tan\alpha_R(\tilde{x}) = \frac{4\sqrt{R_1R_2}(R_2 - R_1)(\tilde{x} + X_0)\sin\theta - (R_2^2 - R_1^2)\tan\theta\sqrt{4(\tilde{x} + X_0)^2 - (R_2 - R_1)^2}}{4\sqrt{R_1R_2}(R_2 + R_1)(\tilde{x} + X_0)\sin\theta\tan\theta + (R_2 - R_1)^2\sqrt{4(\tilde{x} + X_0)^2 - (R_2 - R_1)^2}}. \tag{8}$$

In order to compare the measured shape with the desired hyperbolic shape, we need to calculate the surface height and slope distributions, $y_R(x_R)$ and $\alpha_R(x_R)$ as functions of x_R, rather than $\tilde{x}$ as in Eqs. (6) and (8). This problem is solved by reversing Eq. (6a) to express the positions $\tilde{x}$ in the shifted (but not rotated) coordinate system as a function $\tilde{x}(x_R)$ of the measured positions x_R in the MRC system (x_R, y_R),

$$\tilde{x}(x_R) = \frac{\sec\theta\sqrt{R_1^2 + R_2^2 - 2R_1R_2\cos(2\theta)}\left[(R_2 - R_1)^3 x_R + 2R_1R_2(R_2^2 - R_1^2)\sin\theta\tan\theta\right]}{(R_2 - R_1)^4 - 4R_1R_2(R_1 + R_2)^2\sin^2\theta\tan^2\theta}$$
$$- \frac{4(R_2^2 - R_1^2)\sqrt{R_1R_2}\sin^2\theta\sqrt{x_R^2 + x_R(R_1 + R_2)\cos\theta + R_1R_2}}{\left[R_1^2 - 6R_1R_2 + R_2^2 + (R_1 + R_2)^2\cos(2\theta)\right]\sqrt{R_1^2 + R_2^2 - 2R_1R_2\cos(2\theta)}}. \tag{9}$$

Then, the calculated positions $\tilde{x}(x_R)$ given by Eq. (9) are placed into the expressions (6b) and (8) to calculate the surface height and slope profilers, $y_R(x_R)$ and $\alpha_R(x_R)$, used for verification of the compliance of the measured shape and the specification.

C. Description of elliptical cylinder mirror in the terms of the conjugate parameters

The equations describing shape of an elliptical cylinder x-ray mirror in the MRC system and expressed in terms of R_1,

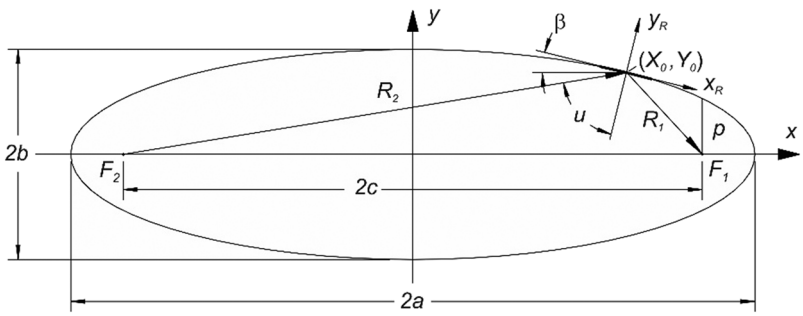

FIG. 3. Ellipse geometry and the major parameters used in the derivations. β is the angle between *x*-axis of the canonic coordinate system of the ellipse and the tangent of the mirror center with the coordinates (X_0, Y_0). Axes $\vec{x}_R$ and $\vec{y}_R$ define the mirror-related Cartesian coordinate system; *a* and *b* are the major and minor semi-axes of the ellipse.

R_2, and θ (Fig. 3) are obtained in the derivations analogous to those outlined in Sec. II C, above[20] (see also Ref. 26 available upon direct request).

In the case of an elliptical mirror, $a = (R_2 + R_1)/2$ and $b = \sin\theta\sqrt{R_2 R_1}$. The coordinates of the mirror pole (X_0, Y_0) are

$$X_0 = \frac{R_2^2 - R_1^2}{2\sqrt{R_2^2 + R_1^2 + 2R_2R_1\cos(2\theta)}}, \tag{10a}$$

$$Y_0 = \frac{R_2R_1\sin(2\theta)}{\sqrt{R_2^2 + R_1^2 + 2R_2R_1\cos(2\theta)}}, \tag{10b}$$

and the rotation angle β is

$$\beta = \arctan\left[\frac{(R_2 - R_1)\tan\theta}{R_2 + R_1}\right]. \tag{11}$$

The resulting expressions for $x_R(\tilde{x})$ and $y_R(\tilde{x})$ [compare with Eqs. (6a) and (6b) for a hyperbolic mirror] are

$$x_R(\tilde{x}) = \frac{\tilde{x}(R_2 + R_1)^2 + Y_0\tan\theta\left(R_2^2 - R_1^2\right) - \sin\theta\tan\theta\sqrt{R_1R_2}(R_2 - R_1)\sqrt{(R_2 + R_1)^2 - 4(\tilde{x} + X_0)^2}}{(R_2 + R_1)\sqrt{(R_2 + R_1)^2 + (R_2 - R_1)^2\tan^2\theta}}, \tag{12a}$$

$$y_R(\tilde{x}) = \frac{\sin\theta\sqrt{R_1R_2}\sqrt{(R_2 + R_1)^2 - 4(\tilde{x} + X_0)^2} + \tilde{x}(R_2 - R_1)\tan\theta - Y_0(R_2 + R_1)}{\sqrt{(R_2 + R_1)^2 + (R_2 - R_1)^2\tan^2\theta}}. \tag{12b}$$

An expression for the surface slope distribution $\alpha_R(\tilde{x})$ for an elliptical mirror [compare with Eq. (7) for a hyperbolic mirror] is

$$\tan\alpha_R(\tilde{x}) = \frac{-4\sin\theta\sqrt{R_1R_2}(R_2 + R_1)(\tilde{x} + X_0) + (R_2^2 - R_1^2)\tan\theta\sqrt{(R_2 + R_1)^2 - 4(\tilde{x} + X_0)^2}}{4\sin\theta\tan\theta\sqrt{R_1R_2}(R_2 - R_1)(\tilde{x} + X_0) + (R_2 + R_1)^2\sqrt{(R_2 + R_1)^2 - 4(\tilde{x} + X_0)^2}}. \tag{13}$$

By reversing Eq. (12a), we express the positions $\tilde{x}$ in the shifted coordinate system of the ellipse as a function $\tilde{x}(x_R)$ of the measured positions x_R in the MRC system (x_R, y_R),

$$\tilde{x}(x_R) = \frac{\sec\theta(R_2 + R_1)\sqrt{R_1^2 + R_2^2 + 2R_1R_2\cos 2\theta}}{(R_2 + R_1)^4 + 4R_1R_2(R_2 - R_1)^2\sin^2\theta\tan^2\theta}\left[x_R(R_2 + R_1)^2 - 2\sqrt{R_1R_2}(R_2 - R_1)\sin\theta\tan\theta\left(\sqrt{R_1R_2} - \sqrt{R_1R_2 - x_R^2 - x_R(R_2 - R_1)\cos\theta}\right)\right]. \tag{14}$$

In order to calculate the surface height and slope distributions, $y_R(x_R)$ and $\alpha_R(x_R)$ of an elliptical mirror as the functions of x_R, one has to place $\tilde{x}(x_R)$ calculated with Eq. (14) into the expressions (12b) and (13) the surface height and slope profilers, $y_R(x_R)$ and $\alpha_R(x_R)$, of the elliptical mirror.

The validity of the analytical expressions given above in this section was verified by comparing the height and slope profiles of the QERLIN SM1 and SM2 mirrors analytically calculated based on the derived expressions, with the profiles numerically generated using the same set of mirror's conjugate parameters.[25,26] For all the expressions, the difference was on the level of inherent precision of the numerical calculations with OriginPro™ software, used for the simulations.

III. SURFACE SLOPE METROLOGY WITH QERLIN SM1 AND SM2 MIRRORS

A. Measurement arrangement

For surface slope metrology with the mirrors, we used the DLTP,[12–14] an electronic autocollimator (AC) and movable pentaprism based surface slope profiler, arranged for measurements with side-facing optics, free of the perturbation of the surface under test (SUT) shape due to gravity sag.

1. Measurement strategy

In order to suppress random noise and instrumental drift error, each measurement run consisted 8 scans in the forward and reversed DLTP scanning directions according to the optimal scanning strategy.[27] To minimize the impact of systematic error, a series of 4 runs: two pairs of runs separated by a tilt of 140 μrad with the substrate flipped in orientation between recording slope traces of the titled pairs, was arranged for each measured trace. Averaging of the measurements carried out at the pitch tilts different by 140 μrad allows us to suppress a periodic systematic error of the DLTP AC with the period of about 280 μrad. By averaging the measurements performed with the optic in two different orientations, direct and flipped, we suppress the part of the systematic error that is even with respect to the reversal of the tangential coordinate. A comprehensive description of the correlation methods developed and used at the XROL for suppression of the measurement random noise and error due to the instrumental drift and systematic effects can be found in Ref. 16.

2. Tangential position alignment

When the mirror is placed on the DLTP for measurements (Fig. 4), the tangential position alignment was determined using both a CCD camera placed behind each end of the substrate (Fig. 5) and looking at the autocollimator signal reflected through the iris diaphragm of the translational pentaprism head and using nulling of the AC signal as it reflected from the edges. The estimated absolute accuracy of the positioning is less than 50 μm.

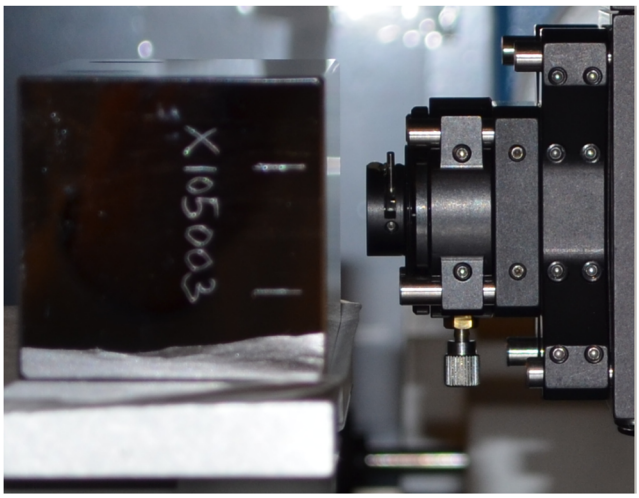

FIG. 4. The mirror SM1 with the serial number seen as placed on the DLTP for surface slope measurements. The iris diaphragm on the left part of the picture is used to collimate the AC light beam. For the measurements with the QERLIN mirrors, the diaphragm orifice was adjusted to 2.5 mm diameter.

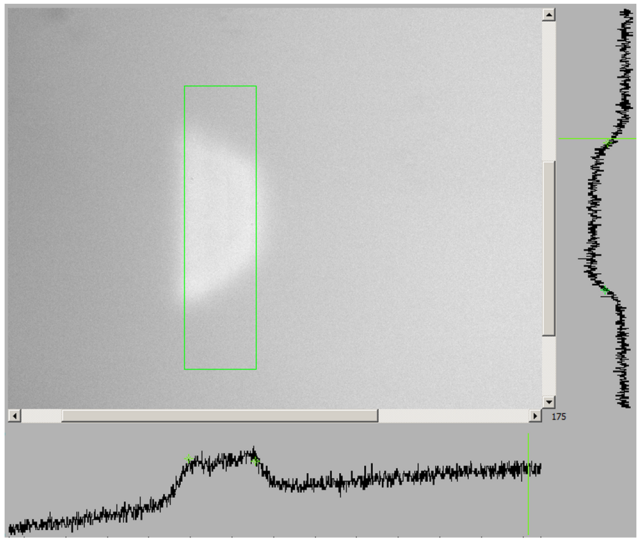

FIG. 5. Positioning of the substrate on the DLTP using a camera placed behind each end of the mirror under measurement. A view of the autocollimator beam through the 2.5 mm iris diaphragm in the front of the DLTP scanning pentaprism, half obscured by the substrate.

3. Aligning direct and flipped measurements

High accuracy positioning of the SUT is also required for reliable averaging of the measurements carried out with the SUT in the direct and flipped orientations.

To obtain an absolute position of the measured trace, with 150 mm specified CA length, the DLTP gantry is scanned over a 170 mm coordinate domain in increments of 0.2 mm. Overscanning provides a record of the position of the substrate

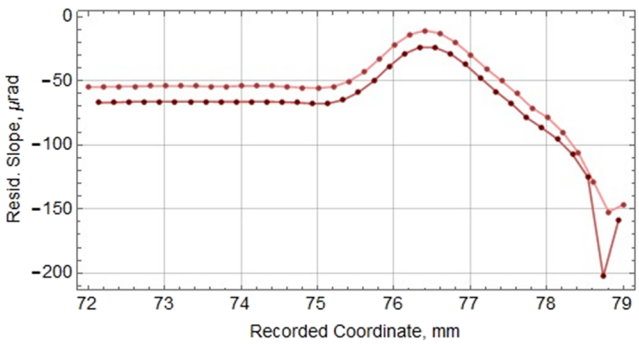

FIG. 6. The SM1 downstream end of the direct and flipped measurements of a tangential slope trace, shown after alignment based on cross-correlation analysis in Fig. 7.

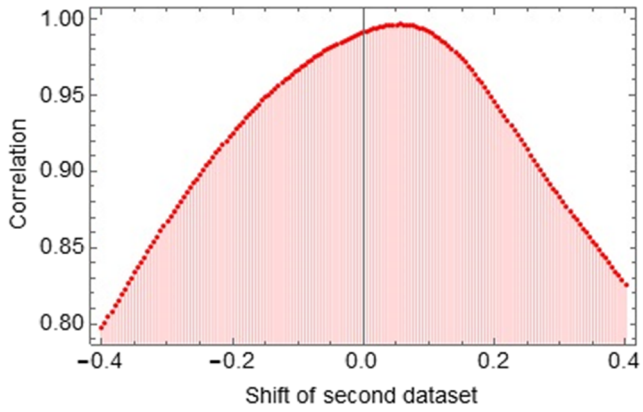

FIG. 7. Plot of the cross-correlation of the direct dataset translated along the coordinates of the flipped dataset, with maximum correlation at a translation of 0.055 mm, used in averaging of the direct and flipped measurements.

with respect to the DLTP gantry coordinates by observing the characteristic surface shape perturbation at the edges of the CA (see Fig. 6). The measurements in Fig. 6 are shown after alignment based on cross-correlation analysis depicted in Fig. 7.

B. Results of the measurements

1. Tangential slope measurements with SM1 mirror

Figure 8(a) shows the surface slope variation along the tangential direction of the hyperbolic SM1 mirror. The trace is the result of averaging 4 runs arranged as discussed in Sec. III A 1. Additionally, the final trace was corrected to account the DLTP systematic error measured in the dedicated experiments described in detail in Ref. 14. The total slope variation along the mirror CA is about 2.1 mrad. With all the precautions applied, the repeatability of the measurements is about 60 nrad (RMS).

The residual, after subtraction of the hyperbolic shape determined with the specified central values of the mirror conjugate parameters in Table I, is depicted in Fig. 8(a). The PV and RMS variations of the residual slope distribution are about 31 μrad and 9.1 μrad, respectively.

2. Tangential slope measurements with SM2 mirror

The measurement result in Fig. 8 presents only one tangential slope trace of two specified for measurements with each mirror along the tangential lines shifted by ±5 mm from the sagittal center. In order to illustrate the approximate invariance of the measured tangential slope distributions on the sagittal shift in these sagittally plane mirrors, Fig. 9 shows the residual surface slope variations along two tangential lines of the elliptical SM2 mirror. Each measurement is also the result of averaging 4 runs arranged as discussed in Sec. III A 1; and the final slope trace was also corrected to additionally account the DLTP systematic error.[14] The total slope variation along the mirror SM2 CA is about 2 mrad.

Similar to the case of the hyperbolic mirror in Fig. 8(b), the residual slope variations in Fig. 9 are the results of detrending the measured slope data with the elliptical shape corresponding to the specified central values of the SM2 mirror conjugate parameters in Table I. The PV variations of the residual slope distributions are about 6.5 μrad.

Because of the dramatic deviation of the slope profiles of SM1 and SM2 mirrors, as measured with the DLTP, from the ideal shapes corresponding to the central values of the specified conjugate parameters, we have also verified the DLTP results via comparison with the measurements with the new OSMS profiler,[15–17] also available at the ALS XROL. The NOM[28,29]-like gantry system of the OSMS is capable of two-dimensional surface slope metrology over the spatial range from the sub-mm scale to the clear aperture. The OSMS gantry system incorporates the custom combined tip, tilt, pitch, and rotation stage. The gantry system and the original data acquisition software of the OSMS are designed[16,17] to support two-dimensional multi-scan measurement runs optimized for automatic suppression and compensation of

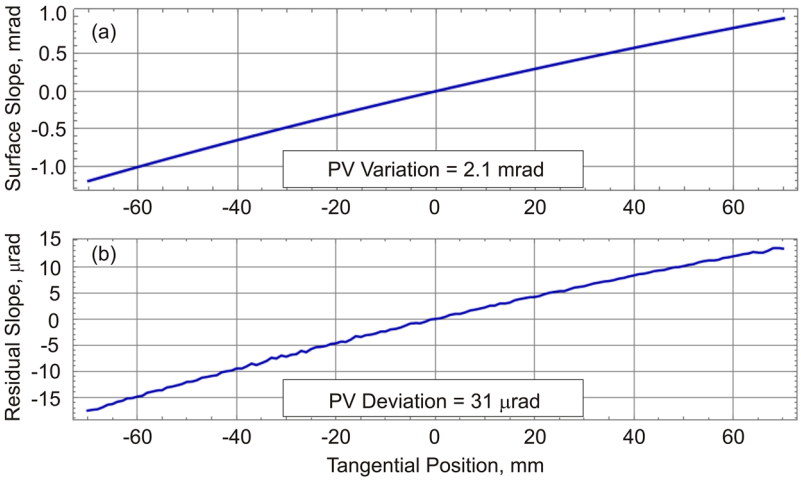

FIG. 8. (a) Surface slope variation along the tangential direction of the hyperbolic SM1 mirror. (b) Residual, after subtraction of the hyperbolic shape determined with the specified central values of the mirror conjugate parameters in Table I. The total slope variation along the mirror CA is about 2.1 mrad. The PV and RMS variations of the residual slope distribution are about 31 μrad and 9.1 μrad, respectively.

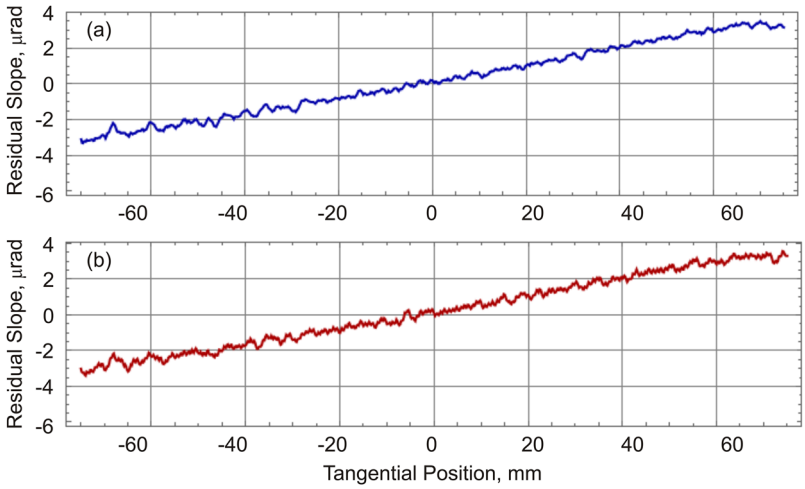

FIG. 9. [(a) and (b)] Residual (after detrending the ideal elliptical shape corresponding to the specified central values of the mirror conjugate parameters in Table I) surface slope distributions of the elliptical SM2 mirror measured along two tangential lines shifted from the sagittal center by ±5 mm. The PV variations of the residual slope distributions are about 6.5 μrad.

instrumental drifts and major angular and spatial systematic errors with different types and arrangements of sensors.

The distinguishing feature of the OSMS profiler is implementation of four electronic autocollimators that allows us to characterize the optics in the side-facing and face-up orientations. With a face-up SUT, we use the OSMS measurement arrangement with the sample-channel AC placed on the carriage and an additional AC in the reference channel for monitoring carriage wobbling in the course of translation.[17] Such an arrangement provides surface slope measurements in the sample channel free of the systematic error due to the variation of the length of the AC optical path.[30,31] To the best of our knowledge, the arrangement of an AC-based surface slope profilometer with a movable, vertically oriented AC and an additional AC in the reference channel was first considered in Ref. 32 and implemented and published in Refs. 15–17 and 33.

The measurements with the OSMS with face-up orientation of the SM1 and SM2 mirrors have confirmed the correctness of the DLTP metrology with the mirrors.

The major conclusion from the performed measurements with the pre-shaped aspherical mirrors SM1 and SM2 is as follows: the surface figures of both mirrors strongly deviate from the ideal shapes determined with the central values of the conjugate parameters, as specified in Table I. Therefore, a more sophisticated analysis of the measured shapes of the mirrors is required in order to understand the compliance of the surface figures of the mirrors with the tolerance specification.

IV. OPTIMIZATION OF THE CONJUGATE PARAMETERS

A. Extension of the method of characteristic functions

Mathematically, the procedure for optimization of the conjugate parameters of a pre-shaped x-ray mirror, described in the present paper, is similar to the method developed at the ALS XROL for optimal tuning of bendable x-ray mirrors (see recent publication[20] and references therein). The idea of the method consists in best fitting the shape error of a bendable mirror with experimentally determined characteristic functions of the mirror benders.[20,34–36]

In the procedure extended here to optimization of the conjugate parameters of a pre-shaped x-ray mirror, the shape error calculated by detrending the measured slope distribution with the ideal shape is fitted with the characteristic functions that are the partial derivatives over the conjugate parameters of the analytical expression describing the desired slope figure of the mirror (see Sec. II). In order to adapt the optimal bending software,[20,35,36] developed at the XROL, the characteristic functions are calculated as normalized differences of the analytically calculated shapes corresponding to a small change of the corresponding conjugate parameter with respect to the specified central values.

Then, with the software, the linear regression analysis method is applied to regress (best fit) the error between the measured and the theoretical slope distributions. The determined vector of adjustments of the conjugate parameters is applied to "tune" the theoretical distribution to best match the measurement.

Because the three conjugate parameters that specify hyperbolic and elliptical mirrors (see Table I) are interdependent, we optimize different combinations of one or two conjugate parameters:

(i) optimization of θ only at the desired central values of R_1 and R_2;
(ii) optimization of R_1 and θ at the desired central values of R_2;
(iii) optimization of R_2 and θ at the desired central value of R_1;
(iv) optimization of R_1, R_2, and θ subject to the conditions $R_2 - R_1 \equiv 2a$ or $R_2 + R_1 \equiv 2a$ (in the case of a hyperbolic or elliptical mirror, respectively);
(v) optimization of R_2, under the condition $R_2 - R_1 \equiv 2a$ or $R_2 + R_1 \equiv 2a$ (in the case of a hyperbolic or elliptical mirror, respectively) and at the desired central value of θ.

As an example of the developed optimization algorithms, we consider the option (iv) in application to a hyperbolic cylinder mirror, where the parameters R_1, R_2, and θ are adjusted under the condition $R_2 - R_1 = R_2^0 - R_1^0 \equiv 2a$. Here, R_1^0, R_2^0, and θ_0 are the central values of the corresponding parameters. This case can be thought of as a spatial translation of the hyperbolic mirror at almost unchanged positions of the object focus of the hyperbolic mirror, F_1, and the common focus of the hyperbolic and elliptical mirrors in the Wolter pair, F_2 (see Fig. 1).

Let us denote α_i and $\alpha(R_1, R_2, \theta, x_i)$ to be the measured and the theoretical slope functions. The desired (ideal) slope distribution $\alpha_0(R_1^0, R_2^0, \theta_0, x_i)$ corresponds to the central, ideal values of the conjugate parameters.

In the case of hyperbolic cylinder mirror, in order to calculate the characteristic functions for fitting R_1 and θ under the condition

$$R_2 - R_1 = R_2^0 - R_1^0 \equiv 2a, \tag{15}$$

we calculate [in addition to the ideal slope distribution: $\alpha_0(R_1^0, R_2^0, \theta_0, x_i)$] the slope distributions

$$\alpha_1(R_1^0 + \delta R_1, R_2^0 + \delta R_1, \theta_0, x_i), \tag{16}$$

and

$$\alpha_2(R_1^0, R_2^0, \theta_0 + \delta\theta, x_i). \tag{17}$$

In Eq. (16), we change the parameter δR_2 by δR_1 in order to account condition (15).

The calculated (shifted) distributions (16) and (17) do not correspond to our usual sequence of measurements for setting a bendable mirror. In the case of tuning the bendable mirrors, we first measure the slope distribution with some initial parameters. This can be thought of as the parameter R_1^0 changed by δR_1. Next, we take the second measurement with the first parameter changed. Finally, we change the second parameter (this can be thought of as the parameter θ_0 changed by $\delta\theta$) and perform the third measurement. This sequence of the measurements helps us to minimize the spurious effect of a possible backlash problem in the mirror bender mechanism. In the case of optimization of the conjugate parameters of the hyperbola, we do not have the backlash problem, and the characteristic functions can be calculated with respect to the ideal hyperbola.

The corresponding characteristic functions to be used for optimization of the conjugate parameters are

$$f_{R_1}(x_i) = \frac{\alpha_1(R_1^0 + \delta R_1, R_2^0 + \delta R_1, \theta, x_i) - \alpha_0(R_1^0, R_2^0, \theta_0, x_i)}{\delta R_1} \tag{18a}$$

and

$$f_\theta(x_i) = \frac{\alpha_2(R_1^0, R_2^0, \theta_0 + \delta\theta, x_i) - \alpha_1(R_1^0, R_2^0, \theta_0, x_i)}{\delta\theta}. \tag{18b}$$

The goal of the optimization is to match the calculated shape to that measured, or in other words, to fit the error with the characteristic functions,

$$\alpha_i - \alpha_0(R_1^0, R_2^0, \theta_0, x_i) \approx \Delta_{R_1} \cdot f_{R_1}(x_i) + \Delta_\theta \cdot f_\theta(x_i) + A_0. \tag{19}$$

The constant (independent of x_i) parameter of fitting A_0 has to be included in order to account for the possible overall tilt difference between the measured and the theoretical slope distributions. After application of linear regression analysis with the three column regression matrix (see, for example, Ref. 20 and references therein), we get a set of the best fit adjustments for the parameters,

$$\Delta_{R1}^*, \Delta_\theta^*, \text{ and } A_0^*. \tag{20}$$

With the asterisk, we separate the estimate from the true value of the parameters.

With the best-fit adjustments (20), we calculated the parameters $\left(R_1^0 + \Delta_{R_1}^*\right)$, $\left(R_2^0 + \Delta_{R_1}^*\right)$, and $\left(\theta_0 + \Delta_\theta^*\right)$ of the best-fit hyperbola,

$$\alpha_i \approx \alpha_0(R_1^0, R_2^0, \theta_0, x_i) + \Delta_{R_1}^* \cdot f_{R_1}(x_i) + \Delta_\theta^* \cdot f_\theta(x_i) + A_0^*, \tag{21a}$$

or

$$\alpha_i \approx \alpha^*(R_1^0 + \Delta_{R_1}^*, R_2^0 + \Delta_{R_1}^*, \theta_0 + \Delta_\theta^*, x_i) + A_0^*. \tag{21b}$$

The optimization algorithm outlined here, as well as other optimization options listed above in this section, was realized in dedicated software developed in the IDL development environment platform. The software allows optimization of the mirror conjugate parameters using linear regression analysis to minimize the RMS variation of the residual slope trace. Then, the predicted conjugate parameters are applied to the analytical equations for the desired mirror shape, presented in Sec. II, to calculate the shape of the ideal hyperbolic or elliptical cylinder mirror best-fit to the measurements. In order to get the best possible set of the new conjugate parameters (corresponding to the minimum possible residual slope error), it can be necessary to apply a few sequential optimization iterations. This is due to the non-exact linearity of the optimization problem. Each next optimization has to use the parameters predicted in the previous iteration as the parameters of the new ideal hyperbola. Practically, in order to optimize the conjugate parameters of a high quality elliptical or parabolic x-ray mirror, we usually need 1 or 2 iterations.

B. Optimal conjugate parameters for SM1 mirror

Table II summarizes the result of the three iterations of optimization of the conjugate parameters of the hyperbolic cylinder mirror SM1 for the ALS QERLIN beamline for four different optimization options. In the table, σ_{PRED} and $\sigma_{ACHIVED}$ are the predicted and achieved residual (after subtraction of the corresponding predicted hyperbolic shape) slope variations (RMS).

In the case of the QERLIN SM1 hyperbolic mirror, the optimization procedure with two variables converges in two iterations (see Table II). The third iteration was performed to check the stability of the result. Optimization of the single parameter θ converges in one iteration. The achieved RMS error is close, but noticeably higher than the specified tolerance of 150 nrad (RMS). Therefore, we can conclude that optimization by adjusting only the grazing angle is almost acceptable. The two-parameter optimizations, when one of

TABLE II. The results of the third optimization run for different optimization options applied to the slope distributions measured with the hyperbolic cylinder mirror SM1. σ_{PRED} and $\sigma_{ACHIVED}$ are the predicted and achieved residual (after subtraction of the corresponding predicted hyperbolic shape) slope variations (RMS). $\Delta^*_{R_1}$, $\Delta^*_{R_2}$, and Δ^*_θ are the deviation of the optimized parameters from the specified central values.

Parameter	Specified/Ideal	(i)[a]	(ii)[b]	(iii)[c]	(iv)[d]
R_1 (mm)	700.00	700.00	697.1156	700.00	697.492 22
R_2 (mm)	1781.97	1781.97	1781.97	1763.017 74	1779.462 22
θ (mrad)	34.906 59	35.418 505 2	35.176 982 05	35.665 209 11	35.240 211 75
σ_{PRED} (μrad)	...	0.163	0.126	0.125	0.126
$\sigma_{\mathrm{ACHIEVED}}$ (μrad)	9.134	0.163	0.126	0.125	0.126
$\Delta^*_{R_1}$ (mm)	±10	...	−2.884	...	−2.508
$\Delta^*_{R_2}$ (mm)	±10	...	...	−18.952	−2.508
Δ^*_θ (mrad)	±0.52	+0.512	+0.270	+0.758	+0.334
Is it within the spec?	...	CLOSE	YES	NO	YES

[a](i) is the optimization of grazing incidence angle θ only at the fixed central values of distances R_1^0 and R_2^0.
[b](ii) is the optimization of R_1 and θ at the fixed central values of distance R_2^0.
[c](iii) is the optimization of R_2 and θ at the fixed central values of distance R_1^0.
[d](iv) is the optimization of R_1 and θ at $R_2 - R_1 = R_2^0 - R_1^0 \equiv 2a$.

the parameters is the grazing angle, lead to almost the same result with RMS error on the level of 125 nrad, below the specified tolerance.

The deviations $\Delta^*_{R_1}$, $\Delta^*_{R_2}$, and Δ^*_θ of the optimized parameters from the central values specified in Table I are presented in the three last rows of Table II. They suggest that the optimization of R_2 and θ at $R_1 = R_1^0$ leads to the values of the parameters unacceptably outside the specified tolerances.

There is one more optimization option realized in our software that is not presented in Table II. We have empirically found that a shift of the mirror center along the ideal hyperbola, determined by the central values of the conjugate parameters, such that the both R_1 and R_2 are decreased by 4.775 mm allows us to get the mirror arrangement with the RMS error close to the specification: 0.190 μrad (RMS). In this case, the new grazing incidence angle is calculated from the condition of the preservation of the value of the "imaginary" semi-axis $b = \sin\theta_0\sqrt{R_2^0 R_1^0}$ corresponding to the ideal hyperbola. The last relation is also applicable to any other point of the same branch of the hyperbola, determined with the set of parameters R_1, R_2, and θ: $b = \sin\theta_0\sqrt{R_2^0 R_1^0} = \sin\theta\sqrt{R_2 R_1}$. Therefore, in the case of the mirror shifted along the ideal hyperbola, the new grazing incidence angle can be found as

$$\theta = \arcsin\left[\sin\theta_0\sqrt{\frac{R_2^0 R_1^0}{R_2 R_1}}\right]. \tag{22}$$

In the case of the mirror shift by 4.775 mm, the corresponding value of the grazing incidence angle is θ = 35.0734 mrad that is within the specified tolerance. Note that optimization of the grazing angle for R_1 and R_2 equally shifted (decreased) by 4.775 mm leads to an RMS error of 0.157 μrad at θ = 35.0793 mrad; larger only by 6 μrad than the non-optimized value.

The selection of the most preferable set of the optimized conjugate parameters among the options (ii) and (iv) in Table II has to be performed via simulation of the mirror performance as a part of the optical schematic of the QERLIN spectrometer. Such simulations are out of the scope of the present paper.

Figure 10 depicts the residual slope distribution of the hyperbolic mirror corresponding to the optimization (ii) in Table II. The residual slope variation is flat with an RMS variation of 126 nrad.

C. Optimal conjugate parameters for SM2 mirror

Here, we use the developed optimization method and software for the optimization of the conjugate parameters

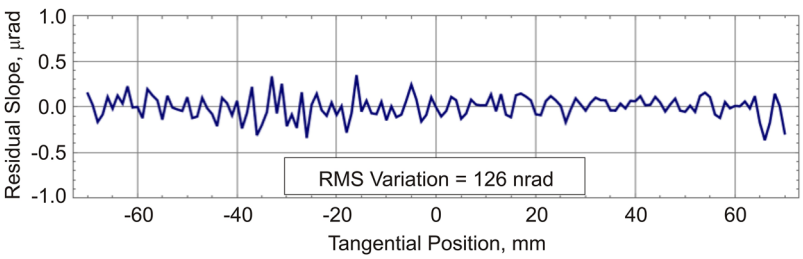

FIG. 10. Residual slope distribution of the hyperbolic mirror SM1 corresponding to the optimization (ii) in Table II. The residual slope variation is flat with the RMS variation of 126 nrad.

TABLE III. The results of the third optimization runs for different optimization options applied to the slope distributions measured with the elliptical cylinder mirror SM2. σ_{PRED} and $\sigma_{ACHIVED}$ are the predicted and achieved residual (after subtraction of the corresponding predicted elliptical shape) slope variations (RMS). $\Delta^*_{R_1}$, $\Delta^*_{R_2}$, and Δ^*_θ are the deviation of the optimized parameters from the specified central values.

Parameter	Specified/ideal	(i)[a]	(ii)[b]	(iii)[c]	(iv)[d]
R_1 (mm)	3600.00	3600.0	3538.56	3600.0	3585.31
R_2 (mm)	1981.97	1981.97	1981.97	2001.24	1996.66
θ (mrad)	34.906 585	35.024 31	34.809 68	35.243 50	35.140 17
σ_{PRED} (μrad)	...	0.128	0.105	0.104	0.104 5
σ_{ACHIEVED} (μrad)	1.885	0.128	0.105	0.104	0.104 5
$\Delta^*_{R_1}$ (mm)	±10	...	−64.44	...	−14.69
$\Delta^*_{R_2}$ (mm)	±10	...	...	+19.27	+14.69
Δ^*_θ (mrad)	±0.52	+0.118	−0.097	+0.337	+0.234
Is it within the spec?	...	YES	NO	NO	NO

[a](i) is the optimization of grazing incidence angle θ only at the fixed central values of distances R_1^0 and R_2^0.
[b](ii) is the optimization of R_1 and θ at the fixed central values of distance R_2^0.
[c](iii) is the optimization of R_2 and θ at the fixed central values of distance R_1^0.
[d](iv) is the optimization of R_1 and θ at $R_2 + R_1 = R_2^0 + R_1^0 \equiv 2a$.

to best fit the measured surface slope distribution for the SM2 elliptical mirror. Similar to the hyperbolic SM1 mirror, we examine different combinations of the regressed parameters listed in Sec. IV A. For some options, we apply a few sequential optimization iterations. Each next optimization uses the parameters predicted in the previous iteration as the parameters of the new ideal ellipse. The parameters predicted in three optimization runs are given in Table III.

In the case of the QERLIN SM2 elliptical cylinder mirror (Table III), the optimization procedure requires two iterations only in the case of regression of R_1 and θ at the central value of the distance R_2^0. In all other cases, it is enough with one iteration. The third iteration was performed to check the stability of the result.

The only optimization that provides the conjugate parameters within the specified tolerances is the optimization option (i) by adjusting only the grazing angle. The resultant RMS error is 128 nrad.

The residual slope trace for the elliptical mirror SM2 after detrending the measured slope distribution with the elliptical shape optimized by regressing the grazing angle only is shown in Fig. 11.

According to the data in Table III, a smaller residual slope error of below 105 nrad (RMS) is possible if the mirror is shifted by 14.69 mm downstream. Although such a shift is significantly out of the specified tolerances, this result is in agreement with slope errors achievable with the empirically predicted shifts of 7.5 mm in the downstream directions, R_1 = 1989.47 mm and

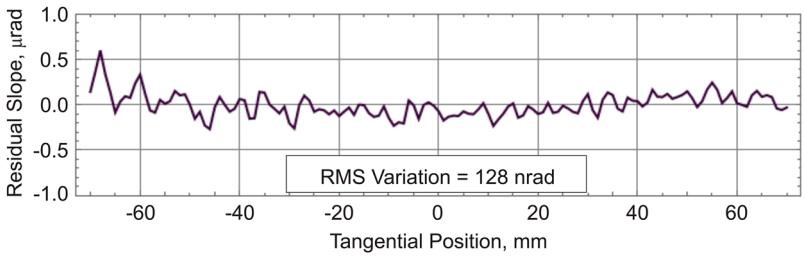

FIG. 11. Residual slope distribution of the elliptical mirror SM2 corresponding to the optimization (i) in Table II. The residual slope variation is flat with the RMS variation of 128 nrad.

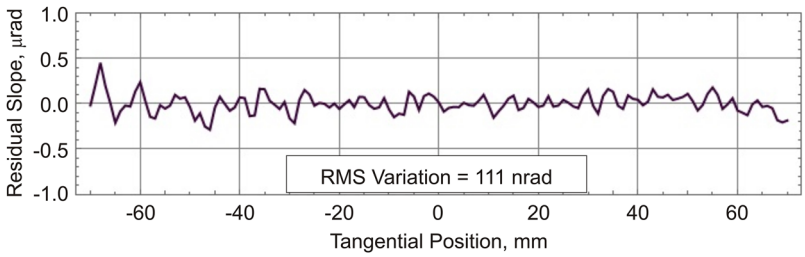

FIG. 12. Residual slope, after subtraction of the elliptical shape, corresponding to the downstream shift of 7.5 mm, R_1 = 1989.47 mm and R_2 = 3592.50 mm, and the grazing angle θ = 35.0837 mrad, optimized for the shift (see also discussion in the text). The RMS variation of the residual slope is 110.6 nrad.

R_2 = 3592.50 mm. In this case, we also optimally adjust the grazing incidence angle, θ = 35.0837 mrad. The corresponding residual slope distribution is shown in Fig. 12. The residual slope variation is 110.6 nrad (RMS).

V. CONCLUSIONS

In the present paper, we have first described an original procedure and dedicated software developed at the ALS XROL for optimization of the beamline performance of the pre-shaped hyperbolic and elliptical mirrors. The optimization consists in minimization of the deviation of the mirror surface slope profile from the desired hyperbolic or elliptical cylinder shape by optimization of the conjugate parameters (distances from the source and image focal points to the mirror center and the corresponding grazing incidence angles) of the mirror beamline application within the specified tolerances. Mathematically, the set of the optimal conjugate parameters is determined from the best fit of the mirror surface shape error with analytically derived fitting functions inherent (characteristic) to the desired mirror shape (hyperbolic or elliptical) defined by the conjugate parameters. The determined optimal conjugate parameters completely define the optimal alignment of the mirror at the beamline that effectively preserves the desired shape of the mirror.

High efficacy of the developed surface slope metrology and data analysis procedures has been demonstrated in the measurements with and performance optimization of the hyperbolic, SM1, and elliptical, SM2, cylinder mirrors fabricated for the ALS QERLIN beamline.

The mirrors were measured at the ALS XROL using original measurement tools and error suppression methods. The accuracy of the measurement is estimated to be on the level of 60 nrad (RMS). For the surface slope metrology with the mirrors, we have used the DLTP[12–14] and verified the results via comparison with that of obtained with the new OSMS,[15–17] both available at the ALS XROL. The measurements suggest that the QERLIN SM1 and SM2 mirrors are fabricated with shapes significantly different from the ideal shapes (corresponding to the central values of the specified conjugate parameters) with the PV deviations of 31 μrad and 6.5 μrad, respectively. Note that the surface slope error specified for the mirrors is <150 nrad (RMS).

Nevertheless, application of the optimization procedure with the dedicated software allows us to prove that the surface shapes of the mirrors are still within the specification given with the tolerances. This means that specification with tolerances must assume post-fabrication global optimization of the beamline geometry for its best performance.

As the necessary foundation for pre- and post-fabrication simulation and optimization, we have provided the analytical expressions for calculation of the hyperbolic and elliptical mirror tangential profiles in the height and slope domain as the functions of the conjugate parameters of the mirrors. We have also outlined the essentials of the optimization algorithm realized in the dedicated software developed at the ALS XROL. Our software applied here for optimization of the QERLIN SM1 hyperbolic and SM2 elliptical mirrors is an indispensable part of our global beamline optimization.

In the case of the QERLIN SM1 and SM2 mirrors, the performed optimization of their conjugate parameters has provided the best-fit desired shapes with the RMS deviation from the measured profiles of ~126 nrad (RMS) and ~111 nrad (RMS) that is well below the specified surface slope error of <150 nrad (RMS).

In this paper, we have used as a figure of merit for the optimization the minimum of the RMS variation of the residual surface slope distribution. However, in the recent publication,[20] it is shown that in the case of optimal tuning of x-ray bendable mirrors, an additional improvement of the mirror beamline performance is obtained in optimization by accounting for the peculiarities of the mirror geometry and x-ray beam intensity distribution. In the case of focusing mirrors, the figure of merit for the tuning is the minimum of the RMS size of the focused beam. The efficacy of the optimization has been demonstrated with examples of optimal tuning of an elliptically bendable cylindrical mirror designed for the ALS micro-diffraction beamline 10.3.2.[20] We plan to extend the method to the optimization of the conjugate parameters of the pre-shape x-ray mirrors. Work in this direction is in progress.

ACKNOWLEDGMENTS

The authors are grateful to Raymond Barrett, Sergey Nikitin, and Howard Padmore for useful discussions. The Advanced Light Source is supported by the Director, Office of Science, Office of Basic Energy Sciences, Material Science Division, of the U.S. Department of Energy under Contract No. DE-AC02-05CH11231 at the Lawrence Berkeley National Laboratory.

REFERENCES

[1]L. Samoylova, H. Sinn, F. Siewert, H. Mimura, K. Yamauchi, and T. Tschentscher, Proc. SPIE **7360**, 73600E/1-9 (2009).

[2]L. Assoufid and T. Rabedeau, Co-Chairs, "X-ray mirrors," in *X-ray Optics for BES Light Source Facilities, Report of the Basic Energy Sciences Workshop on X-Ray Optics for BES Light Source Facilities*, edited by D. Mills

and H. Padmore, Co-Chairs (U.S. Department of Energy, Office of Science, Potomac, MD, 2013), pp. 118–129, http://science.energy.gov/~/media/bes/pdf/reports/files/BES_XRay_Optics_rpt.pdf.
[3]V. V. Yashchuk, L. Samoylova, and I. V. Kozhevnikov, Proc. SPIE **9209**, 92090F/1-19 (2014).
[4]V. V. Yashchuk, L. Samoylova, and I. V. Kozhevnikov, Opt. Eng. **54**(2), 025108/1-13 (2015).
[5]D. Cocco, Photonics **2**(1), 40–49 (2015).
[6]See https://als.lbl.gov/als-u/ for ALS-U.
[7]S. Kevan, Chair, "ALS-U: Solving scientific challenges with coherent soft x-rays," in *Workshop Report on Early Science Enabled by the Advanced Light Source Upgrade* (ALS, LBNL, Berkeley, CA, 2017), https://als.lbl.gov/wp-content/uploads/2017/08/ALS-U-Early-Science-Workshop-Report-Full.pdf.
[8]M. Idir and V. V. Yashchuk, Co-Chairs, "Optical and x-ray metrology," in *X-ray Optics for BES Light Source Facilities, Report of the Basic Energy Sciences Workshop on X-Ray Optics for BES Light Source Facilities*, edited by D. Mills and H. Padmore, Co-Chairs (U.S. Department of Energy, Office of Science, Potomac, MD, 2013), pp. 44–55, http://science.energy.gov/~/media/bes/pdf/reports/files/BES_XRay_Optics_rpt.pdf.
[9]V. V. Yashchuk, N. A. Artemiev, I. Lacey, W. R. McKinney, and H. A. Padmore, Proc. SPIE **9206**, 920601/1-19 (2014).
[10]V. V. Yashchuk, N. A. Artemiev, I. Lacey, W. R. McKinney, and H. A. Padmore, Opt. Eng. **54**(10), 104104/1-14 (2015).
[11]Y.-D. Chuang, C. Anderson, M. Benk, K. Goldberg, D. Voronov, T. Warwick, V. Yashchuk, and H. A. Padmore, AIP Conf. Proc. **1741**, 050011/1-5 (2016).
[12]V. V. Yashchuk, S. Barber, E. E. Domning, J. L. Kirschman, G. Y. Morrison, B. V. Smith, F. Siewert, T. Zeschke, R. Geckeler, and A. Just, Nucl. Instrum. Methods Phys. Res., Sect. A **616**(2-3), 212–223 (2010).
[13]S. K. Barber, G. Y. Morrison, V. V. Yashchuk, M. V. Gubarev, R. D. Geckeler, J. Buchheim, F. Siewert, and T. Zeschke, Opt. Eng. **50**(5), 053601/1-10 (2011).
[14]I. Lacey, N. A. Artemiev, E. E. Domning, W. R. McKinney, G. Y. Morrison, S. A. Morton, B. V. Smith, and V. V. Yashchuk, Proc. SPIE **9206**, 920603/1-11 (2014).
[15]I. Lacey, J. Adam, G. Centers, G. S. Gevorkyan, S. M. Nikitin, B. V. Smith, and V. V. Yashchuk, Proc. SPIE **10385**, 103850G/1-13 (2017).
[16]V. V. Yashchuk, G. Centers, G. S. Gevorkyan, I. Lacey, and B. V. Smith, Proc. SPIE **10612**, 106120O/1-23 (2018).
[17]I. Lacey, K. Anderson, G. P. Centers, G. S. Gevorkyan, T. Nicolot, B. V. Smith, and V. V. Yashchuk, Proc. SPIE **10760**, 1076002/1-20 (2018).
[18]H. Wolter, Ann. Phys. **445**(10), 94–114 (1952).
[19]H. Wolter, Ann. Phys. **445**(10), 286–295 (1952).
[20]V. V. Yashchuk, I. Lacey, and W. R. McKinney, Proc. SPIE **10761**, 1076108/1-23 (2018).
[21]L. J. P. Ament, M. van Veenendaal, T. P. Devereaux, J. P. Hill, and J. van den Brink, Rev. Mod. Phys. **83**, 705–767 (2011).
[22]K. Lieutenant, T. Hofmann, C. Schulz, M. V. Yablonskikh, K. Habicht, and E. F. Aziz, J. Electron Spectrosc. Relat. Phenom. **210**, 54–65 (2016).
[23]See https://www.maxiv.lu.se/accelerators-beamlines/beamlines/veritas/ for MAX-IV beamline VERITAS.
[24]See http://tpsbl.nsrrc.org.tw/bd_page.aspx?lang=en&port=41A&pid=1044 for TPS beamline 41A: Soft X-ray Scattering.
[25]V. V. Yashchuk, S. M. Nikitin, I. Lacey, and W. R. McKinney, "Hyperbolic cylinder x-ray mirror: Basic equations in the terms of the conjugate parameters," in *Light Source Beam Light Note LSBL-1320* (Advanced Light Source, Berkeley, 2017).
[26]V. V. Yashchuk, I. Lacey, W. R. McKinney, S. M. Nikitin, and T. Warwick, "Elliptical cylinder x-ray Mirror: Basic equations in the terms of the conjugate parameters," in *Light Source Beam Light Note LSBL-1346* (Advanced Light Source, Berkeley, 2017).
[27]V. V. Yashchuk, Rev. Sci. Instrum. **80**, 115101/1-10 (2009).
[28]F. Siewert, T. Noll, T. Schlegel, T. Zeschke, and H. Lammert, AIP Conf. Proc. **705**, 847–850 (2004).
[29]F. Siewert, J. Buchheim, T. Zeschke, M. Störmer, G. Falkenberg, and R. Sankari, J. Synchrotron Radiat. **21**, 968–975 (2014).
[30]R. D. Geckeler and A. Just, Proc. SPIE **7077**, 70770B/1-12 (2008).
[31]R. Geckeler, A. Just, M. Krause, and V. V. Yashchuk, Nucl. Instrum. Methods Phys. Res., Sect. A **616**, 140–146 (2010).
[32]V. V. Yashchuk, "Sub-microradian surface slope metrology at the ALS optical metrology laboratory and around the world," in Oral Presentation at the First Meeting on Development of a New Optical Surface Slope Measuring System–OSMS-I, ALS, Berkeley, March 26, 2010.
[33]S. Qian and M. Idir, Proc. SPIE **9687**, 96870D/1-10 (2016).
[34]O. Hignette, A. Freund, and E. Chinchio, Proc. SPIE **3152**, 188–199 (1997).
[35]W. R. McKinney, J. L. Kirschman, A. A. MacDowell, T. Warwick, and V. V. Yashchuk, Opt. Eng. **48**(8), 083601/1-8 (2009).
[36]W. R. McKinney, V. V. Yashchuk, K. A. Goldberg, H. Howells, N. A. Artemiev, D. J. Merthe, and S. Yuan, Proc. SPIE **8141**, 81410K/1-14 (2011).